EPR, ^1H and ^{13}C ENDOR, ^{14}N ESEEM, and X-ray Crystallographic Studies of Oxovanadium(IV) Bis((1*R*)-3-(heptafluorobutyryl)camphorate): A Catalyst for Asymmetric Hetero Diels-Alder Reactions

Antonio Togni,*,†,‡ Günther Rist,† Grety Rihs,† and Arthur Schweiger§

Contribution from the Physics Department and Central Research Services, CIBA-GEIGY Ltd., P.O. Box, CH-4002 Basel, Switzerland, and Laboratory of Physical Chemistry, Swiss Federal Institute of Technology (ETH), CH-8092 Zürich, Switzerland. *Received August 11, 1992*

Abstract: Oxovanadium(IV) bis((1*R*)-3-(heptafluorobutyryl)camphorate) (**1**), an active catalyst for asymmetric hetero Diels-Alder reactions, is trimeric in the solid state. $(\mathbf{1})_3$ crystallizes in the cubic system, space group $P2_13$, with four molecules in the unit cell of dimension a = 21.352(2) Å. The core of the cluster is constituted by a planar V_3O_3 ring with alternating long (2.14(1) Å) and short (1.57(1) Å) V-O distances. Each vanadium atom is slightly distorted octahedrally coordinated. The adducts of **1** with benzaldehyde and *N*-benzylidene-benzylamine, two potential substrates for the catalytic reaction, have been studied by EPR, ^1H and ^{13}C ENDOR, and ^{14}N ESEEM pulsed techniques in frozen toluene solutions (10-20 K). It was found that benzaldehyde adopts an η^1 coordination mode trans to the oxo ligand, whereas the imine coordinates in cis position to the oxo ligand. Spectroscopic evidence is presented that the angle V-O-C in the aldehyde adduct lies in the expected range of 130-140°, typical for an η^1 geometry.

Introduction

There is currently great interest in the use of Lewis acids as catalysts in organic synthesis.[1] Several chiral, optically active Lewis acids have been shown to be highly enantioselective catalysts in a variety of transformations. In particular, derivatives of Ti(IV), Sn(II), and Sn(IV), and B have found application in, e.g., aldol,[2] Diels-Alder,[3] ene,[4] and Darzens reactions.[5] In most cases, the catalyst is formed in situ from a suitable precursor and a chiral ligand. Often, and despite its successful application, reliable information about the very nature of the catalytically active species and its complexes with the substrate is not available.

We recently reported[6] that the complex oxovanadium(IV) bis((1*R*)-3-(heptafluorobutyryl)camphorate) (**1**) is an effective catalyst for the hetero Diels-Alder reaction.[7] Thus, condensation of an aldehyde (the hetero dienophile component) with an activated diene of type **2** is achieved at low temperature in the presence of 5 mol % of **1** (eq 1). The primary cycloaddition product is not

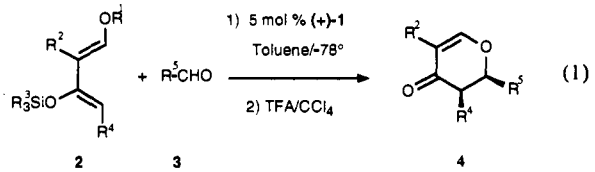

2 3 4 (1)

up to 85 % e.e.
98-99 % diastereoselectivity

isolated but is converted in situ upon protonolysis, giving 5,6-γ-dihydropyrones **4**. Enantioselectivities of up to 85% were thereby obtained. Diastereoselectivities in the range of 98-99% for 5,6-cis-configurated products were in general observed, indicative of a (2 + 4) cycloaddition mechanism.[8] **1** still consitutes a rare example of an non-d^0 transition-metal complex that can be exploited as a catalytically active Lewis acid in such types of reactions. The title compound shows a peculiar specificity for the substrate combination aldehyde/1-alkoxy-3-(silyloxy)butadiene, other substrates being either unreactive or giving very low selectivities. In particular, imines, as the hetero dienophile components (isoelectronic to aldehydes), are completely unreactive under V(IV) catalytic conditions.

As established by molecular weight determination in solution, **1** is monomeric.[6] If one reasonably assumes a square pyramidal

Chart I

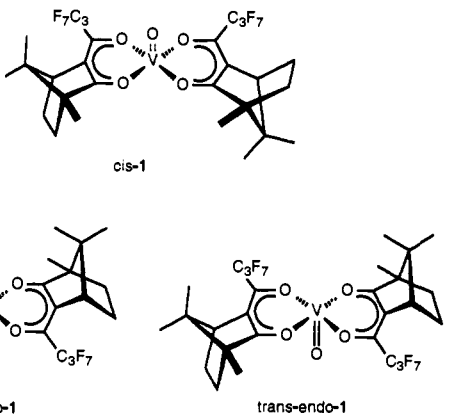

coordination geometry around vanadium, as it is found for oxovanadium bis(1,3-diketonate) complexes,[9] then three descrete diastereoisomeric forms of **1** are possible, as illustrated in Chart I. As previously discussed,[6] we have indications that the material we used as a catalyst is constituted by one single stereoisomeric form, namely *cis*-**1**.

In order to (1) clarify structural aspects of the free catalyst and (2) try to understand the different reactivities of the substrates aldehyde and imine, X-ray crystallographic and EPR/ENDOR studies were carried out. The results from these studies are the subject of the present report.

† CIBA-GEIGY Ltd.
‡ Present address: Laboratory of Inorganic Chemistry, Swiss Federal Institute of Technology (ETH), CH-8092 Zürich, Switzerland.
§ ETH Zürich.

(1) *Selectivity in Lewis Acid Promoted Reactions*; Schinzer, D., Ed.; NATO Series; Kluwer: Dordrecht, The Netherlands, 1989.
(2) See, e.g.: Kobayashi, S.; Uchiro, H.; Fujishita, Y.; Shiina, I.; Mukaiyama, T. *J. Am. Chem. Soc.* **1991**, *113*, 4247-4252, and references cited therein.
(3) See, e.g.: (a) Furuta, K.; Shimizu, S.; Miwa, Y.; Yamamoto, H. *J. Org. Chem.* **1989**, *54*, 1481-1483. (b) Corey, E. J.; Loh, T.-P. *J. Am. Chem. Soc.* **1991**, *113*, 8966-8967, and references cited therein.
(4) See, e.g.: Mikami, K.; Terada, M.; Nakai, T. *J. Am. Chem. Soc.* **1990**, *112*, 3949-3954, and references cited therein.
(5) Corey, E. J.; Choi, S. *Tetrahedron Lett.* **1991**, *32*, 2857-2860.
(6) Togni, A. *Organometallics* **1990**, *9*, 3106-3113.
(7) Boger, D. L.; Weinreb, S. N. *Hetero Diels-Alder Methodology in Organic Synthesis*; Academic Press: San Diego, CA, 1987.
(8) (a) Larson, E. R.; Danishefsky, S. *J. Am. Chem. Soc.* **1982**, *104*, 6458-6460. (b) Larson, E. R.; Danishefsky, S. *Tetrahedron Lett.* **1982**, *23*, 1975-1978.
(9) (a) Dodge, R. P.; Templeton, D. H.; Zalkin, A. *J. Chem. Phys.* **1961**, *35*, 55-67. (b) Hon, P.-K.; Belford, R. L.; Pfluger, C. E. *J. Chem. Phys.* **1965**, *43*, 3111-3115. (c) Hon, P.-K.; Belford, R. L.; Pfluger, C. E. *J. Chem. Phys.* **1965**, *43*, 1323-1333.

0002-7863/93/1515-1908$04.00/0

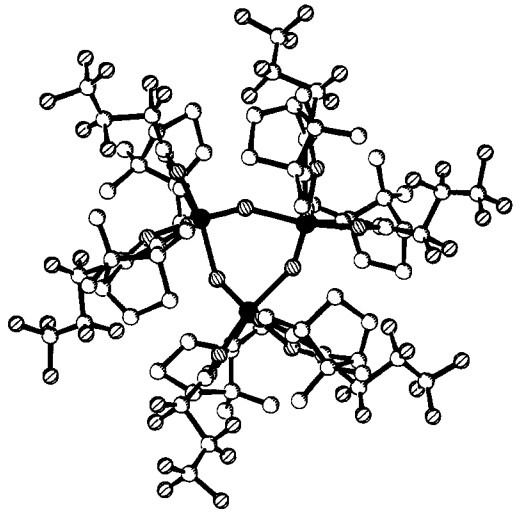

Figure 1. Schakal drawing of $(1)_3$ along the crystallographic C_3-axis. Oxygen atoms are tightly hatched and fluorine atoms are loosely hatched.

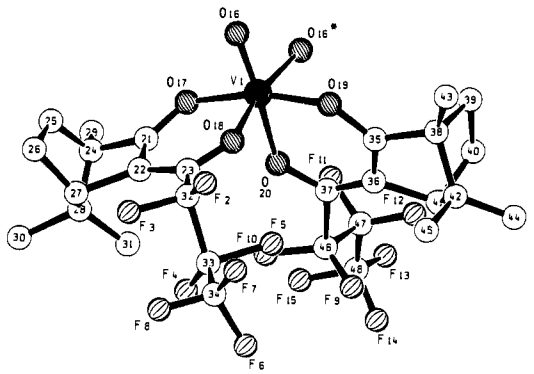

Figure 2. Monomeric unit of $(1)_3$ showing the adopted atom numbering scheme. O(16)* belongs to the next unit in the trimer.

Results and Discussion

Solid-State Structure of Oxovanadium(IV) Bis(3-(heptafluorobutyryl)camphorate). Due to its high solubility in organic solvents, suitable crystals of **1** could only be obtained by slow evaporation of a concentrated CH_2Cl_2 solution at room temperature (for details, see the Experimental Section).

Selected interatomic distances and angles are given in Table I. The overall geometry of the complex is shown in the Schakal[10] representation of Figure 1, and the adopted atom numbering scheme is depicted in Figure 2.

Surprisingly, **1** was found to be *trimeric* in the solid state, and Figure 3 details the core of the cluster. The three monomeric units of the cluster turn out to be equivalent and are connected by a crystallographic C_3 symmetry axis. Each vanadyl oxygen atom acts as a bridging ligand between two vanadium atoms. Thus, the inner core of the cluster is constituted by a six-membered V_3O_3 cyclic fragment with alternating short (1.57(1) Å) and long (2.14(1) Å) V–O distances. The V_3O_3 ring is almost perfectly planar. The bridging oxygen atoms are situated 0.02 Å from the plane defined by the vanadium atoms. Whereas dinuclear complexes[11] and a recently described tetranuclear species,[12] as well as polymeric linear chain compounds[13] containing oxo-bridges between V-atoms bearing organic ligands are known, to the best of our knowledge $(1)_3$ appears to be the first example of such a trinuclear oxo-bridged cluster. Each vanadyl oxygen in $(1)_3$ can be considered to act as a Lewis base, and thus the observed aggregation to form the trimer is an expression of the Lewis amphotericity of vanadyl bis(1,3-diketonate) complexes.[14] The V–O–V angle in dimeric singly bridged complexes is usually quite large and often approaches 180°.[11] The tendency for linearity of such fragments is also reflected by the rather wide V–O–V angle observed in the cyclic complex $(1)_3$ (151.5(8)°).

The local geometry at each vanadium atom is best described as distorted octahedral. The unexpected but salient structural feature revealed by the X-ray study concerns the relative position of the two chelating ligands. They are found to lie in two planes nearly perpendicular to one another (the angle between the planes of the chelating six-membered rings is 89°) as a result of the bridging position of the oxo ligands, whose relative position is best viewed as cis. The aggregation to form the trimeric structure in the solid state has thus lead to an isomerization in the coordination sphere of vanadium similar to that encountered for addition complexes of $VO(acac)_2$ with, e.g., amines[15] (see also discussion

Table I. Selected Interatomic Distances[a] and Angles[a] for **1**

Bond Distances (Å)			
V–O(16)	1.57(1)	V–O(16*)	2.14(1)
V–O(17)	1.96(1)	V–O(18)	1.81(1)
V–O(19)	1.84(1)	V–O(20)	1.84(1)
O(17)–C(21)	1.31(2)	O(18)–C(23)	1.24(3)
O(19)–C(35)	1.39(2)	O(20)–C(37)	1.27(2)
C(21)–C(22)	1.38(3)	C(22)–C(23)	1.46(3)
C(35)–C(36)	1.36(3)	C(36)–C(37)	1.33(3)
C(23)–C(32)	1.40(4)	C(37)–C(46)	1.67(3)
(C–F)	1.38(3)	V–V	3.16(1)
Bond Angles (deg)			
O(16)–V–O(16*)	88.5(6)	O(16*)–V–O(17)	92.5(5)
O(16*)–V–O(18)	168.2(5)	O(16*)–V–O(19)	87.2(5)
O(16*)–V–O(20)	85.9(6)	O(16)–V–O(17)	91.1(7)
O(16)–V–O(18)	102.1(7)	O(16)–V–O(19)	105.0(7)
O(16)–V–O(20)	170.7(6)	O(17)–V–O(18)	92.4(6)
O(17)–V–O(19)	163.9(6)	O(17)–V–O(20)	81.7(6)
O(18)–V–O(19)	85.2(6)	O(18)–V–O(20)	84.3(7)
O(19)–V–O(20)	82.2(6)	V–O(16)–V*	151.5(8)
V–O(17)–C(21)	121(1)	V–O(18)–C(23)	133(1)
V–O(19)–C(35)	131(1)	V–O(20)–C(37)	136(1)
O(17)–C(21)–C(22)	130(2)	C(21)–C(22)–C(23)	118(2)
O(18)–C(23)–C(22)	125(2)	O(19)–C(35)–C(36)	127(2)
C(35)–C(36)–C(37)	121(2)	O(20)–C(37)–C(36)	117(2)
C(22)–C(23)–C(32)	125(2)	O(18)–C(23)–C(32)	109(2)
C(36)–C(37)–C(46)	119(2)	O(20)–C(37)–C(46)	121(2)

[a] Numbers in parentheses are estimated standard deviations in the least significant digits.

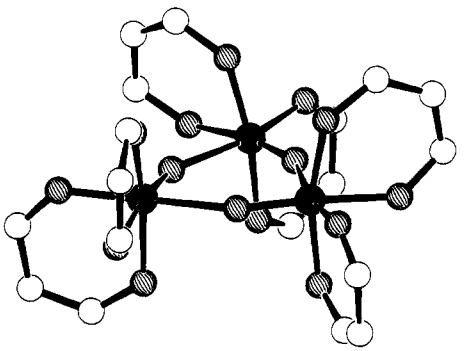

Figure 3. Inner core of the cluster, emphasizing the coordination geometry around the vanadium atoms. Oxygen atoms are hatched.

(10) Keller, E. *Schakal88*; A Program for the Graphic Representation of Molecular and Crystallographic Models; Kristallographisches Institut der Universität Freiburg, D-7200 Freiburg, Germany, 1988.

(11) See, e.g.: (a) Li, X.; Soo Lah, M.; Pecoraro, V. L. *Inorg. Chem.* **1988**, *27*, 4657–4664. (b) Yamada, S.; Katayama, C.; Tanaka, J.; Tanaka, M. *Inorg. Chem.* **1984**, *23*, 253–255. (c) Kojima, A.; Okazaki, K.; Ooi, S.; Saito, K. *Inorg. Chem.* **1983**, *22*, 1168–1174. (d) Edwards, A. J.; Slim, D. R.; Guerchais, J. E.; Sala-Pala, J. *J. Chem. Soc., Dalton Trans.* **1977**, 984–986.

(12) Hills, A.; Hughes, D. L.; Leigh, G. J.; Sanders, J. R. *J. Chem. Soc., Chem. Commun.* **1991**, 827–829.

(13) Serrette, A.; Carroll, P. J.; Swager, T. M. *J. Am. Chem. Soc.* **1992**, *114*, 1887–1889.

(14) The Lewis basicity of the oxygen atom in vanadyl(salen) complexes (V(IV)) has been demonstrated by the complexes' abilities to form adducts with Sn(IV) species. See: (a) Cashin, B.; Cunningham, D.; Gallagher, J. F.; McArdle, P.; Higgins, T. *Polyhedron* **1989**, *8*, 1753–1755. (b) Cashin, B.; Cunningham, D.; Gallagher, J. F.; McArdle, P.; Higgins, T. *J. Chem. Soc., Chem. Commun.* **1989**, 1445–1446.

Chart II

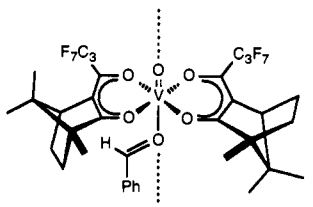

5

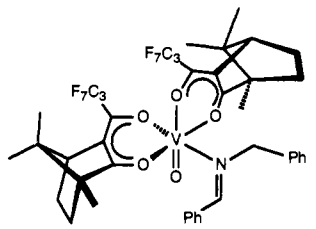

6

of the *N*-benzylidene–benzylamine adduct of **1**, below). One of the two heptafluorobutyryl oxygen atoms is now in an axial position, trans to the oxo ligand, whereas the two stronger donor ligands in the equatorial plane are trans to each other. The observed absolute configuration at the vanadium center is [*OC*-6-33-Δ].[16]

Electron Paramagnetic Resonance (EPR) and Nuclear Magnetic Resonance (NMR). EPR and NMR spectra of **1** in toluene solution with and without addition of benzaldehyde or *N*-benzylidene–benzylamine, respectively, were recorded in order to get a first insight into the geometry and the stability of the adduct complexes (for a proposed structure of the adducts, see Chart II).

The hyperfine coupling constants of the vanadyl nuclear spin of the complexes **1**, **5**, and **6** in solution and frozen solution are collected in Table II. The direction z is oriented coaxially with the V=O vector, whereas the directions x and y are identical with the idealized in-plane O–V–O axes. The changes of the hyperfine coupling constant for the imine adduct with respect to **1** are 2–7 times larger than for the aldehyde adduct. The unpaired electron in **1** is located in an in-plane d_{xy} orbital. The decrease in hyperfine coupling constants in adduct **6** is therefore indicative of stronger in-plane bonds and suggests a reorganization of the in-plane ligands, where one of the oxygens is replaced by the imine nitrogen. This conjecture is supported by the hyperfine and g values estimated with the help of the linear ligand additivity rules put forward by Chasteen.[17] The appropriate values for complex **6**, calculated from the coupling constants of complex **1** and using the parameters for 2,2′-bipyridine, are included in Table II. They show the expected trend. The experimental shifts are even somewhat larger than the calculated ones, presumably because the linear additivity rules do not account for the axial ligand. The smaller changes in hyperfine coupling constants for **5** can be accounted for if one assumes an axial coordination of the aldehyde, keeping in mind that the four in-plane oxygens are stronger donors than the aldehyde. However, for an unequivocal assignment of the plausible adduct geometries, ENDOR and electron spin–echo experiments have been carried out.

The adducts **5** and **6** were also investigated by ^{1}H NMR in the presence of a 10-fold excess of aldehyde and imine, respectively. In these experiments the ^{1}H NMR resonances of the uncomplexed donor molecules are broadened because of chemical exchange with the paramagnetic site, where the ligand nuclear spins interact with the spin of the unpaired electron. The NMR resonance half-width

Table II. Vanadium Hyperfine Coupling Constants (10^{-4} cm^{-1}) and g Values for **1**, **5**, and **6**

	complex		
	1	**5**[a]	**6**[a,b]
a (isotropic), solution	102.5	101.5 (1.0%)	98.1 (4.3%) [98.8]
a, frozen solution[c]	101.3	100.0 (1.2%)	97.4 (3.8%)
A_z	173.8	173.3 (0.3%)	168.9 (2.8%)[d] [171.0]
$^1/_2$ $(A_x + A_y)$	65.0	63.4 (2.5%)	61.7 (5.1%)
$^1/_2$ $(A_x - A_y)$[e]	*f*	2.3	*f*
g_0 (isotropic), solution	1.975	1.975	1.976 [1.975]
g_z	1.946	1.947	1.949
$^1/_2$ $(g_x + g_y)$	1.989	1.993	1.987

[a] Numbers in parentheses indicate the changes of the hyperfine coupling constants between free complex **1** and the adducts **5** and **6**. [b] Numbers in square brackets are values calculated on the basis of the linear ligand additivity rules (see text and ref 17). [c] a (frozen solution) = $^1/_3$ $(A_x + A_y + A_z)$. [d] Mean value; depending on freezing cycle, small splittings due to two or several sites. [e] Orthorhombic component with the assumption $g_x = g_y$. [f] No orthorhombic component observed at X-band.

at half-height ($1/T_2$) of a nuclear spin interchanging between a diamagnetic (lifetime t_D) and a paramagnetic (lifetime t_P) state is given by:[18]

$$1/T_2 = 1/t_D\{(at_P/2)^2/[1 + (at_P/2)^2]\}$$

In the limit of strong paramagnetic pulses, $(at_P/2)^2 \gg 1$; therefore, the parameter T_2 is a direct measure of the lifetime t_D. ENDOR experiments (vide infra) have shown that the hyperfine coupling constants of both the aldehyde and imine protons are of the order of megahertz. At a given time, all vanadyl complexes in solution are present as adducts. For both strong and weak paramagnetic pulses, the increase of the NMR line width is therefore equivalent to a decrease of t_D and t_P by the exchange process. The broadening for the imine and methylene ^{1}H-resonance due to paramagnetic species is of the order of $1/T_2$ = 1.0–1.5 Hz, part of which may be due to intermolecular dipolar coupling. The broadening of the aldehyde proton resonance is approximately 10 Hz. Within the strong pulse limit and the molar ratios noted above, broadenings of these sizes correspond to lifetimes of the order of 0.1 and 0.01 s for the imine and aldehyde adducts, respectively. This observation is again compatible with the reorganization of the ligand sphere in the imine complex.

Electron Nuclear Double Resonance—^{13}C ENDOR. A pulsed ^{13}C ENDOR study of carbonyl-^{13}C-labeled benzaldehyde (Ph–^{13}CHO) has been carried out to determine the binding site of this potential sixth ligand for **1** (cis or trans to the vanadyl oxygen). In the Mims–ENDOR scheme used in these experiments,[19] the relative change of the echo amplitude I_{echo} under the rf pulse is given by the ENDOR efficiency $F_{ENDOR} = {}^1/_2|[I_{echo}(\text{rf off}) - I_{echo}(\text{rf on})/I_{echo}(\text{rf off})]| = {}^1/_2 \sin^2(\pi A^C \tau)$.[20] F_{ENDOR} depends on the actual hyperfine splitting A^C and on the time τ between the first two $\pi/2$ microwave pulses; it reaches its maximum for $\tau = (2n + 1)/2A^C$ and is 0 for $\tau = n/A^C$, $n = 0, 1, 2, \cdots$.

Frozen solution ^{13}C ENDOR spectra have been measured at different B_0 field positions, marked in the EPR spectrum in Figure 4. The assignment of the transitions in this figure to the corresponding magnetic quantum numbers m^V_I of the vanadium nucleus is based on a positive vanadium hyperfine coupling.[17] The EPR spectrum was recorded with the FID-detected hole burning technique;[21] this method avoids distortions caused by the ESEEM (electron spin–echo envelope modulation) effect, which are often observed in echo-detected EPR spectra.[22,23] The ENDOR

(15) For example, the adduct of 4-phenylpyridine with $VO(acac)_2$ was characterized by X-ray diffraction; see: Caira, M. R.; Haigh, J.M.; Nassimbeni, L. R. *Inorg. Nucl. Chem. Lett.* **1972**, *8*, 109–112.
(16) Sloan, T. E. *Top. Stereochem.* **1981**, *12*, 1–36.
(17) Chasteen, N. D. In *Biological Magnetic Resonance*; Berliner, L. J., Reuben, J., Eds.; Plenum Press: New York, 1981; Vol. 3, pp 53–119.
(18) Kreilick, R. W. In *NMR of Paramagnetic Molecules*; La Mar, G. N., Horrocks, W. D., Jr., Holm, R. H., Eds.; Academic Press: New York, 1973; p 598.
(19) Mims, W. B. *Proc. Royal Soc.* **1965**, *A283*, 452–457.
(20) Gemperle, C.; Schweiger, A. *Chem. Rev.* **1991**, *91*, 1481–1505.
(21) Wacker, T.; Sierra, G.; Schweiger, A. *Isr. J. Chem.* In press.
(22) Schweiger, A.; Ernst, R. R. *J. Magn. Reson.* **1988**, *77*, 512–523.

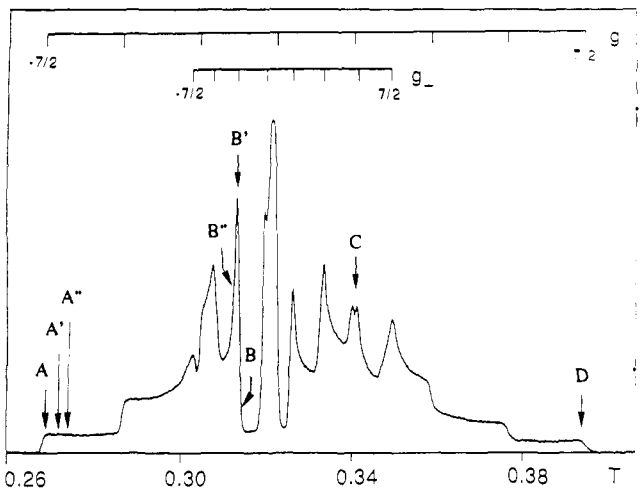

Figure 4. Frozen solution EPR spectrum of the benzaldehyde adduct of **1** in toluene, recorded with the FID-detected hole burning technique. Letters mark observer positions used in the pulsed ENDOR and ESEEM experiments. For the assignment of the m_I values, a positive ^{51}V hyperfine coupling constant has been assumed.

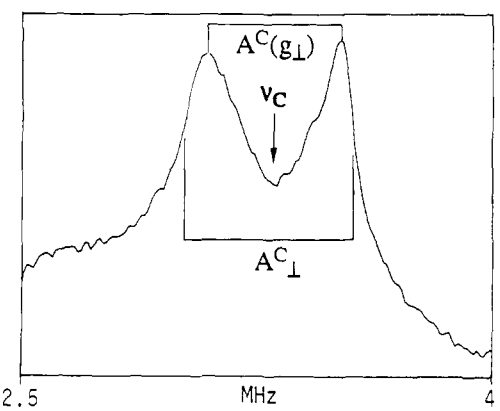

Figure 5. Pulsed Mims-type ^{13}C ENDOR spectrum of the benzaldehyde adduct of **1**. B_0 field position B, ν_C: Zeeman frequency of the ^{13}C nucleus, τ = 800 ns, T = 20 K.

spectrum at the high-field end of the $g_\perp$ feature with $m^V{}_I = -3/2$ (position B, τ = 800 ns) shown in Figure 5 represents a powder average of orientations close to the main coordination plane of **1**[24] (the corresponding $g_\parallel$ feature with $m^V{}_I = -3/2$ is shifted to lower field only by about 7.6 mT). This observer position is used to minimize contributions of out-of-plane orientations in the closer vicinity of the aforementioned plane. The spectrum consists of two peaks with first-order ENDOR frequencies $\nu^C{}_{ENDOR} = \nu_C \pm A^C/2$ symmetric about the Zeeman frequency ν_C = 3.28 MHz of the ^{13}C nucleus. The small line width in this spectrum indicates that the hyperfine splitting A^C is about the same for all orientations of $\boldsymbol{B}_0$ in the complex plane. The ^{13}C hyperfine tensor is therefore assumed to be axially symmetric with an $|A^C{}_\perp|$ value of 0.56 MHz (perpendicular to the V–^{13}C axis), represented by the maximum splitting observed in the spectrum.

Figure 6a shows the ^{13}C ENDOR spectrum recorded at the $g_\parallel$ feature with $m^V{}_I = -7/2$ (low-field end of the EPR spectrum, at half height of the first plateau of the signal, position A). It represents the hyperfine splittings with $\boldsymbol{B}_0$ along the complex normal (parallel to the V=O bond direction). The signal-to-noise ratio is quite poor, since both the EPR signal intensity at this field position and the intensity of the stimulated echo recorded with τ = 500 ns (optimum ENDOR efficiency) are weak. The spectrum consists of two pairs of narrow lines symmetric about ν_C = 2.78 MHz. The peak-to-peak splitting of 1.03 MHz corresponds to the ^{13}C hyperfine coupling $A^C(g_\parallel)$ normal to the main coordination plane. The pair of lines with a splitting of only 0.21 MHz is assigned to a second benzaldehyde molecule hydrogen bonded to the V=O fragment, again showing the Lewis-basic character of the vanadyl oxygen atom (V–^{13}C distance ca. 5.7 Å). The same hyperfine splittings have also been observed at position C ($g_\parallel$ feature with $m^V{}_I = 1/2$ overlaps with the $g_\perp$ feature with $m^V{}_I = 5/2$) and position D ($g_\parallel$ feature with $m^V{}_I = 7/2$).

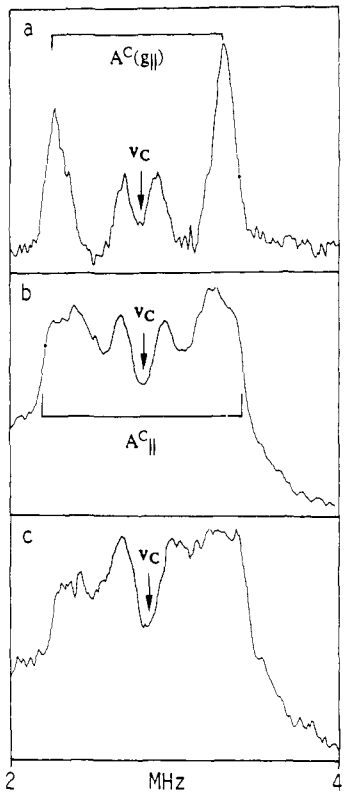

Figure 6. Pulsed Mims-type ^{13}C ENDOR spectra of the benzaldehyde adduct of **1** with $\boldsymbol{B}_0$ close to the complex normal. ν_C: Zeeman frequency of the ^{13}C nucleus, τ = 500 ns, T = 20 K. (a) $\boldsymbol{B}_0$ field position A. (b) $\boldsymbol{B}_0$ field position A′. (c) $\boldsymbol{B}_0$ field position A″.

Figures 6b and c show the ^{13}C ENDOR spectra measured at observer positions shifted to higher fields by ΔB_0 = 3 mT (position A′) and 5 mT (position A″), respectively. In both cases, a relevant broadening of the lines with the large hyperfine coupling is observed. Such a broadening is expected when the direction of the $A^C{}_\parallel$ principal axis parallel to V–^{13}C bond direction does not coincide with the $g_\parallel$ principal axis, since, with increasing field strengths, orientations with $\boldsymbol{B}_0$ in the closer vicinity of the complex normal become involved in the ENDOR experiment (reduced orientation selectivity). Thus, for $\Delta B_0 > 0$, orientations with both $A^C > A^C(g_\parallel)$ and $A^C < A^C(g_\parallel)$ will contribute to the spectrum. A maximum splitting of 1.21 MHz is found for a shift to higher B_0 fields by ΔB_0 = 3 mT. We assume that this splitting (indicated in Figure 6b) is caused by paramagnetic species for which $\boldsymbol{B}_0$ is oriented along $A^C{}_\parallel$.

The signs assumed for the principal values of the ^{13}C hyperfine tensor ($A^C{}_\parallel > 0$, $A^C{}_\perp < 0$) are valid for a predominantly dipolar coupling. To check this assignment, a ^{13}C ENDOR spectrum has been measured with a field setting *between* the $g_\parallel$ and $g_\perp$ features of $m^V{}_I = -3/2$ (position B″). For the two cases where $A^C{}_\perp > 0$ and $A^C{}_\perp < 0$ (in both cases $A^C{}_\parallel$ is assumed to be positive; a negative sign for $A^C{}_\parallel$ would result in an unreasonably large $|a^C|$), a hyperfine splitting $|A^C| > |A^C{}_\perp|$ and $|A^C| < |A^C{}_\perp|$, respectively, is expected. The latter inequality was verified experimentally. The observed splitting of the peak maxima drops from $|A^C|$ = 0.44 ($A^C(g_\perp)$ in Figure 5) to $|A^C|$ = 0.34 MHz in going from observer position B to position B″. This corroborates the signs chosen for the principal values of the ^{13}C hyperfine tensor.

The data obtained from the ^{13}C ENDOR experiments can only be unequivocally accounted for if one assumes that *benzaldehyde is bonded to the vacant axial position of* **1**. For a benzaldehyde

(23) Goldfarb, D.; Kevan, L. *J. Magn. Reson.* **1988**, *76*, 276–286.
(24) Rist, G.; Hyde, J. H. *J. Chem. Phys.* **1970**, *52*, 4633–4643.

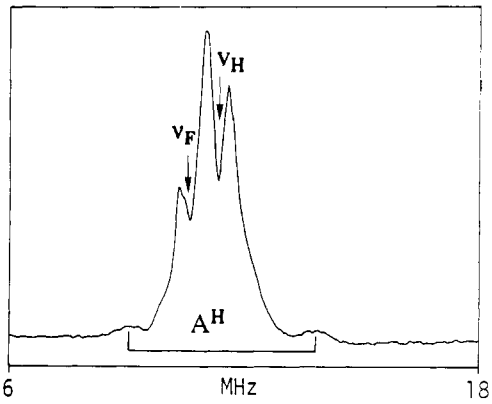

Figure 7. Pulsed Mims-type ^{1}H ENDOR spectrum of the D_5C_6–CHO adduct of **1**. B_0 field position A. ν_H and ν_F denote the Zeeman frequencies of the proton and the fluorine nuclei, respectively.

ligand bonded equatorially to the vanadyl fragment and again assuming $A^C_{\parallel} > |A^C_{\perp}|$,[25,26] the spectrum with $\boldsymbol{B}_0$ in the main coordination plane would cover the full frequency range $\nu_C - A^C_{\parallel}/2 \leq \nu_{ENDOR} < \nu_C + A^C_{\parallel}/2$, whereas in the spectrum with $\boldsymbol{B}_0$ along the complex normal, two narrow peaks with a maximum splitting determined by $A^C_{\perp}$ were to be expected, a situation that fully conflicts with the experimental results.

The principal axis of the largest (positive) value of $A^C_{\parallel}$ of the ^{13}C hyperfine tensor (coinciding with the V–C axis) includes an angle (O_{ald}—V—C) of 10–20° with the V=O bond axis, thus resulting in a bent configuration of the V—O=C fragment. Under the assumption that the point dipole model with $A^C_{\parallel} - a^C = 2g\beta_e g_C \beta_n / hr^3$ is valid,[25] the V—C distance is calculated to be 3.20 Å (the isotropic hyperfine coupling is found to be close to 0, $a^C = 0.03$ MHz). ^{13}C hyperfine coupling constants very close to the ones found in this work have been reported for methanol coordinated in axial position to the VO^{2+} ion.[26] Knowing the angle O_{ald}—V—C and the two distances V—C and C=O (typically ca. 1.24 Å), it is possible to apply simple trigonometry (law of cosines) to evaluate the angle V—O=C and the distance V—O_{ald}, respectively. These are found to amount to 140° and 2.15 Å, respectively, for a value of 15° for the angle mentioned above. From a structural point of view, the angle found for the V—C=O fragment falls into the typical range of 130–140° encountered in complexes containing an η^1-coordinated carbonyl compound (aldehyde, ketone, or ester).[27] This geometry is due to an interaction between the anti lone pair on the oxygen atom and the metal center (mainly σ-type donation).[28] Very wide angles (>170°) have been found only for ester carbonyl coordinated to a metal. Such a geometry would imply a significant π-donation of the oxygen, involving both its lone pairs, thus indicating a much higher Lewis acidity of the metal fragment. Furthermore, the distance of the benzaldehyde oxygen from the vanadium atom of 2.15 Å is in good agreement with M–O bond lengths found in crystallographically characterized complexes.[27] These are for transition metals typically less than 2.2 Å.

^{1}H ENDOR. ^{1}H ENDOR spectra of the adduct of **1** with benzaldehyde-d_5 (D_5C_6–CHO) in deuterated toluene have been recorded in order to gather information about the relative position of the aldehyde proton. The ENDOR transitions of this nucleus

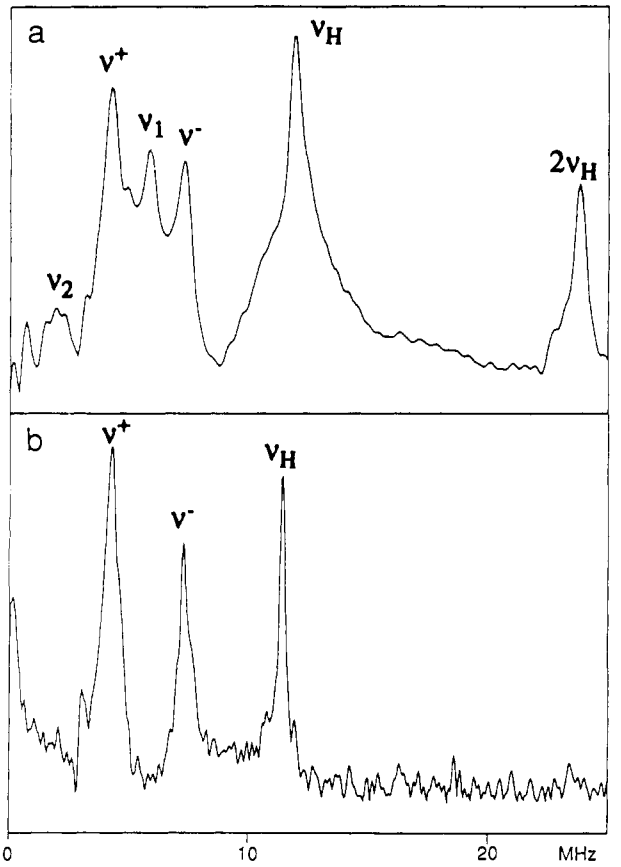

Figure 8. Two- and three-pulse ^{14}N ESEEM spectra of the *N*-benzylidene–benzylamine adduct of **1**, B_0 field position A, $T = 20$ K. (a) Two-pulse magnitude spectrum. (b) Three-pulse magnitude spectrum.

with a hyperfine splitting of $A^H = 4.7$ MHz (containing both dipolar and isotropic contributions) could only be observed at position A, with $\boldsymbol{B}_0$ parallel to $g_{\parallel}$ (Figure 7). From a single hyperfine splitting, however, the V–H distance could not be evaluated. The size of this hyperfine splitting is, nevertheless, compatible with the proposed model.

^{14}N Electron Spin–Echo Envelope Modulation Experiments (^{14}N ESEEM). The aim of the ^{14}N ESEEM studies was to establish whether the model compound *N*-benzylidene–benzylamine, which has been previously used in unsuccessful catalytic experiments,[6] is bonded cis or trans to the vanadyl fragment of **1**. Two- and three-pulse ^{14}N ESEEM measurements have been carried out at field positions A, B′, and D. Spectra recorded at position A and position B′ are shown in Figures 8 and 9, respectively.

One has to remember that the short microwave pulses (10 and 20 ns) reduce the orientation selectivity. Consequently, all the transitions with frequencies containing the strongly orientation-dependent nuclear quadrupole interaction in first order will be broadened. A similar dispersion of the resonance frequencies also occurs for a hyperfine tensor with a large dipolar part. Due to the instrumental deadtime, such broad features are usually not observable in an ESEEM spectrum. We therefore consider only ESEEM frequencies that contain the quadrupole interaction in first order and assume the nitrogen hyperfine tensor to be isotropic.

In order to facilitate the discussion of the measured spectra, we briefly summarize the expressions for the frequencies occurring in the ESEEM experiment. Analytical expressions for two- and three-pulse ESEEM of a spin system ($S = {}^1/_2$, $I = 1$) and a quadrupole coupling, small compared to the hyperfine interaction, have been reported by Mims.[29] In a three-pulse ESEEM experiment, three nuclear transition frequencies for each m_S manifold (two transitions with $\Delta m_I = 1$ and one transition with $\Delta m_I = 2$) contribute to the spectrum. Note that the labeling of the energy

(25) Atherton, N. M.; Shackleton, J. F. *Chem. Phys. Lett.* **1984**, *103*, 302–304.
(26) Mustafi, D.; Makinen, M. W. *Inorg. Chem.* **1988**, *27*, 3360–3368.
(27) A table of bonding parameters for the fragment M–O–C in X-ray characterized complexes containing η^1-coordinated aldehydes, ketones, and esters is given as supplementary material.
(28) This type of interaction is supported by many X-ray crystallographic works on aldehyde–Lewis acid complexes (see table in supplementary material). For theoretical studies of such complexes, see: (a) Reetz, M. T.; Hüllmann, M.; Massa, W.; Berger, S.; Rademacher, P.; Heymanns, P. *J. Am. Chem. Soc.* **1986**, *108*, 2405–2408. (b) LePage, T. J.; Wiberg, K. B. *J. Am. Chem. Soc.* **1988**, *110*, 6642–6650. (c) Loncharich, R. J.; Schwartz, T. R.; Houk, K. N. *J. Am. Chem. Soc.* **1987**, *109*, 14–23. (d) Delbecq, F.; Sautet, P. *J. Am. Chem. Soc.* **1992**, *114*, 2446–2455.
(29) Mims, W. B. *Phys. Rev.* **1972**, *B5*, 2409–2419.

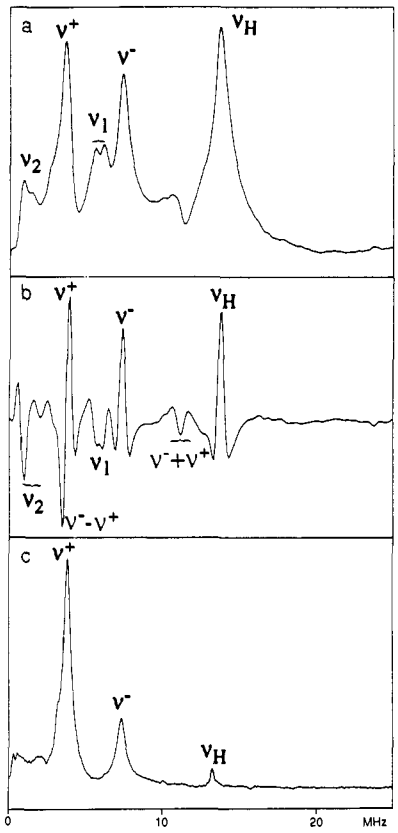

Figure 9. Two- and three-pulse ^{14}N ENDOR spectra of the *N*-benzylidene–benzylamine adduct of **1**, B_0 field position of B′, T = 20 K. (a) Two-pulse magnitude spectrum. (b) Two-pulse cosine-transform spectrum. Prior to transformation the ESEEM pattern is tapered with a shifted hanning window. (c) Three-pulse magnitude spectrum.

levels by m_I, used for convenience, is strictly correct only if the high-field approximation is valid. In the two-pulse experiment, also combinations of these frequencies occur. The four Δm_I = 1 frequencies ν_a, ν_b ($m_S = {}^1/_2$), and ν_c, ν_d ($m_S = -{}^1/_2$), up to first order in the isotropic hyperfine interaction, are given by:[30]

$$\begin{aligned} &m_S = {}^1/_2,\ m_I\colon\ 0 \leftrightarrow 1; && \nu_a = a^N/2 - \nu_N + {}^3/_2Q' \\ &m_S = {}^1/_2,\ m_I\colon\ -1 \leftrightarrow 0; && \nu_b = a^N/2 - \nu_N - {}^3/_2Q' \\ &m_S = -{}^1/_2,\ m_I\colon\ -1 \leftrightarrow 0; && \nu_c = a^N/2 + \nu_N + {}^3/_2Q' \\ &m_S = -{}^1/_2,\ m_I\colon\ 0 \leftrightarrow 1; && \nu_d = a^N/2 + \nu_N - {}^3/_2Q' \end{aligned} \quad (2)$$

where ν_N is the nitrogen Zeeman frequency with $a^N/2 > \nu_N > 0$; $Q' = |Q|$ is the quadrupole interaction in first order with the quadrupole tensor Q (principal values $Q_1 = K(\eta - 1)$, $Q_2 = -K(\eta + 1)$, $Q_3 = 2K$, quadrupole coupling constant $K = e^2qQ/4h$, asymmetry parameter η), and l is the unit vector along B_0.

In the three-pulse ESEEM experiment, only the two overtone frequencies[31]

$$\nu^+ = \nu_a + \nu_b = a^N - 2\nu_N \qquad \nu^- = \nu_c + \nu_d = a^N + 2\nu_N \quad (3)$$

are free of quadrupole interactions in first order. In the two-pulse ESEEM experiments, the combination frequencies (with negative amplitudes), for which the first-order quadrupole contributions are cancelled, are given by

$$\begin{aligned} &\nu_a + \nu_d = a^N \qquad \nu_b + \nu_c = a^N \qquad \nu_c - \nu_a = 2\nu_N \\ &\nu_d - \nu_b = 2\nu_N \qquad \nu^- + \nu^+ = 2a^N \qquad \nu^- - \nu^+ = 4\nu_N \end{aligned} \quad (4)$$

The intensities of the transitions in eqs 3 and 4 are strongly dependent on the magnetic field strength.[33,34] In the ESEEM literature, the expression $\nu^\pm = 2[(a^N/2 \mp \nu_N)^2 + K^2(3 + \eta^2)]^{1/2}$ is often used to describe the overtone frequencies.[32-36] A thorough discussion about the validity of this formula has been given by Singel and co-workers.[33,34]

We now assign the features observed in the ESEEM experiments, starting with the three-pulse spectra shown in Figures 8b (B_0 along the complex normal, position A) and 9c (B_0 in the main coordination plane, position B′). The peak at the proton Zeeman frequency marked by ν_H represents weakly coupled matrix protons and is of no interest in the following discussion. The two peaks below 10 MHz are assigned to the overtone transitions ν^+ and ν^- in the two m_S manifolds. The shift of these frequencies as a function of the observer field B_0 to lower (ν^+) and higher (ν^-) values is about *twice* the change in ^{14}N Zeeman frequency ν_N predicted by eq 3 (position A, ν_N = 0.83 MHz, ν^+ = 4.22 MHz, ν^- = 7.28 MHz; position D, spectrum not shown, ν_N = 1.21 MHz, ν^+ = 3.67 MHz, ν^- = 8.00 MHz). The deviation of this shift from $2\Delta\nu_N$ found for the low-frequency transition ν^+ is caused by the ν_N dependence of the second-order quadrupole interaction, which is larger for the $m_S = {}^1/_2$ than for the $m_S = -{}^1/_2$ manifold. Although the observer position in Figure 8b is set at the extreme low-field end of the EPR spectrum, the orientation selectivity seems not to be high enough for the observation of fundamental frequencies. This might be caused by the short microwave pulses used in the ESEEM experiments.

In the two-pulse ESEEM spectra shown in Figure 8a (B_0 along the complex normal, position A) and 9a,b (B_0 in the main coordination plane, position B′), the peak at the proton Zeeman frequency and the sum peak at twice this frequency are marked by ν_H and $2\nu_H$, respectively. In Figure 8a the nitrogen region is dominated by three peaks. These represent the two overtone transitions ν^+ and ν^-, with the same frequencies as observed in the corresponding three-pulse experiment, and a third peak at ν_1 = 5.89 MHz, assigned to the combination frequencies ($\nu_a + \nu_d$) and ($\nu_b + \nu_c$). The remaining resonances free of quadrupole interactions in first order (eq 4) are hidden in the absorptions of the matrix protons ($\nu^- + \nu^+$) and in the low-frequency flank of the ν^+ resonance ($\nu^- - \nu^+$). The peak at frequency ($\nu_d - \nu_b$, $\nu_c - \nu_a$) is probably represented by the feature marked by ν_2. A similar situation is found in Figure 9a. The splitting of the ν_1 feature into a doublet may be caused by a small anisotropy of the hyperfine coupling.

The higher resolution of the deadtime-reconstructed cosine-transform spectrum shown in Figure 9b allows one to assign all the frequencies of eqs 3 and 4. Besides the two positive peaks ν^+ and ν^-, negative peaks assigned to ν_2, $\nu^- - \nu^+$, ν_1, and $\nu^- + \nu^+$ are also observed.

The isotropic hyperfine interaction is calculated with the formula $a^N \approx [(\nu^-)^2 - (\nu^+)^2]/8\nu_N$. For the imine nitrogen, we find a^N = 5.30 MHz (position A) and a^N = 5.14 MHz (position B′). The similarity of these data for largely different B_0 field orientations confirms that the anisotropic part of the hyperfine coupling is very small.

The large isotropic hyperfine interaction of the nitrogen demonstrates that *the imine ligand is bonded cis to the vanadyl fragment*. A trans coordination can be ruled out, since there is no overlap between the vanadium $3d_{xy}$ orbital carrying the unpaired electron and the orbitals of an axially coordinated nitrogen. Hyperfine coupling constants between 4.5 and 7.6 MHz, measured with ENDOR[37,38] and ESEEM,[35,36,39-42] have been reported for

(30) Schweiger, A. *Struct. Bonding (Berlin)* **1982**, *51*, 1–119.

(31) We use the expression "overtone" [See: (a) Tycko, R.; Opella, S. J. *J. Am. Chem. Soc.* **1986**, *108*, 3531–3532. (b) Tycko, R.; Opella, S. J. *J. Chem. Phys.* **1987**, *86*, 1761–1774. (c) Garroway, A. N.; Miller, J. B. *J. Magn. Reson.* **1989**, *82*, 591–596.], rather than "double quantum", for the transitions between the outer two ^{14}N levels in order to distinguish them from transitions where two quanta are involved.

(32) Astashkin, A. V.; Dikanov, S. A.; Tsvetkov, Y. D. *J. Struct. Chem.* **1984**, *25*, 45–55.

(33) (a) Cosgrove, S. A.; Singel, D. J. *J. Phys. Chem.* **1990**, *94*, 8393–8396. (b) Cosgrove, S. A.; Singel, D. J. *J. Phys. Chem.* **1990**, *94*, 2619–2623.

(34) (a) Flanagan, H. L.; Singel, D. J. *J. Chem. Phys.* **1988**, *89*, 2585–2586. (b) Flanagan, H. L.; Singel, D. J. *J. Chem. Phys.* **1987**, *87*, 5606–5616.

(35) Astashkin, A. V.; Dikanov, S. A.; Tsvetkov, Y. D. *J. Struct. Chem.* **1985**, *26*, 363.

(36) Reijerse, E. J.; Shane, J.; de Boer, E.; Höfer, P.; Collison, D. *Proc. 2nd Workshop on ESR in Disordered Systems*; Bulgaria, 1991.

Scheme I

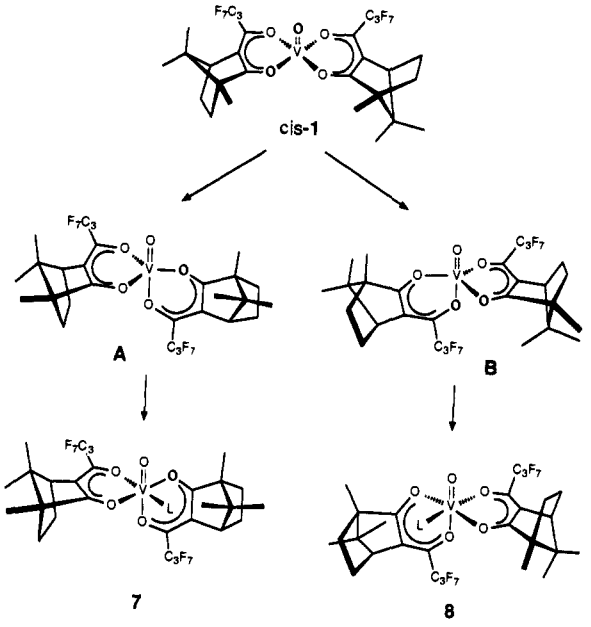

a number of vanadyl complexes with equatorially coordinated nitrogen donor ligands. One of the possible diastereoisomeric forms of the adduct is depicted as structure **6**.

The reasons for the formation of complexes of type **6**, i.e., isomerization upon addition of a sixth ligand, still remain obscure. From a mechanistic point of view, one has to invoke a Berry pseudorotation[43] of the pentacoordinated **1**[44] from a square pyramidal (sp) to a trigonal bipyramidal (tbp) geometry. This motion moves one of the two weaker-bonded ligands (i.e., the oxygen belonging to the perfluoroacyl group) into an axial position. The addition of a ligand L, occuring in the equatorial plane of the complex, may be guided by steric and/or electronic factors. Two of the four diastereotopic pathways of this process, starting from the cis form of **1**, are illustrated in Scheme I. Note that the octahedral complexes **7** and **8** differ only in their absolute configuration at the vanadium stereogenic center (they are epimeric). Unfortunately, such stereochemical differences cannot be identified by EPR/ENDOR techniques. Nevertheless, one has to keep in mind that the adduct studied is probably a mixture of different diastereoisomers. A similar process must be responsible for the now diastereoselective formation of the trimeric form of **1** observed in the solid state (a single configuration is detected, vide supra).

Conclusions

To the best of our knowledge, oxovanadium(IV) bis(1*R*-3-(heptafluorobutyryl)camphorate) (**1**) so far constitutes the only example of vanadyl(IV) complexes bearing chelating monoanionic ligands that adopts a trimeric structure in the solid state. In $(\mathbf{1})_3$ the local coordination geometry at each vanadium atom does not correspond to the one that would result from the addition of a sixth ligand to the axial free coordination site, as is the case for the benzaldehyde adduct. Thus, the structure of $(\mathbf{1})_3$ does not offer any clue as to the actual configuration of **1** in solution.

Table III. Crystal Data and Details of Refinement of **1**

chemical formula	$C_{84}H_{84}F_{42}O_{15}V_3$
fw	2284.34
crystal size, mm	0.45 × 0.32 × 0.15
crystal system	cubic
space group	$P2_13$ (No. 198)
a, Å	21.352(2)
V, Å^3	9735(2)
Z	4
molecular symmetry	C_3
d(calc), g/cm^3	1.558
data collection instrument	Philips PW1100
radiation (λ, Å)	Mo Kα (0.709 26)
monochromator	graphite
F(000)	4620
μ, cm^{-1}	12.2
t, °C	22
2θ range from data collection, deg	6–40
scan time, s	≤42
scan width, deg	1.4
no. of reflns collected	5041
no. of unique reflns	1642
no. of reflections with $I > 3\sigma(I)$	823
no. of variables	198
structure solution	Patterson method
refinement	full-matrix least-squares
residuals: R; R_w	0.104; 0.119
weighting scheme	$w = 1/\sigma^2(\lvert F_o\rvert)$
max. residual electron density, e/Å^3	1.12

This work demonstrates the effectiveness of pulsed EPR techniques in determining subtle features related to the coordination sphere of paramagnetic, catalytically active transition-metal complexes. It has been shown that the adducts of **1** with benzaldehyde and *N*-benzylidene–benzylamine adopt different coordination geometries. Whereas the aldehyde, as expected, occupies the free coordination site trans to the oxo ligand, addition of the imine occurs in a cis fashion. Whether or not this observation correlates with the lack of reactivity of the latter in hetero Diels–Alder reactions in the presence of **1** is still an open question.

Although the spectroscopic data strongly support a bent V–O–C arrangement in the benzaldehyde complex, a precise determination of the coordination geometry could be achieved only by an X-ray crystallographic study. The only derivative that could be obtained in a crystalline form is the adduct with 2-methoxybenzaldehyde, but attempts to grow single crystals have been so far frustrated.

Experimental Section

X-ray Crystallography. Table III provides a summary of the pertinent crystallographic data. Crystals of **1** were obtained from CH_2Cl_2 solutions by slow and *complete* evaporation of the solvent at room temperature. A bulk crystalline material reproducibly formed in round-bottomed flasks as a dark crust by the time almost all solvent had diffused through a needle applied to a serum cap closing the crystallization vessel. Dark brown, platelet-like crystals could be detached from this bulk material and used for preliminary Weissenberg photographs. It was found that these crystals in general had rather low scattering powers. The best one, a crystal of approximate dimensions 0.45 × 0.32 × 0.15 mm^3, was glued at the tip of a MARK glass fiber using ARALDIT RAPID, covered with a thin film of the same glue, and then used for data collection. Intensity data $(+h,+k,+l)$ were gathered by the $\omega/2\theta$ scan method. For ca. 80% of the data collection time, there was no significant intensity variation for three standard reflections measured every 2 h. Afterwards, an increasing decay was observed; therefore, no absorption correction was applied. The structure was solved using the program SHELX 86.[45]

The low number of observed reflections with $I > 3\sigma(I)$ did not allow us to refine all atoms anisotropically (only vanadium was refined). Hydrogen atoms could not be localized. The perfluorinated alkyl chains were found to be disordered. Thus, the isotropic thermal parameters B for, e.g., the fluorine atoms vary from 4.3(3) to 9.2(4) Å^2. The C–F bond distances fluctuate over a rather wide range (1.25(3)–1.54(3) Å) and appear to be in part unrealistic. This observation seems to apply to a number of compounds described in the literature and containing such fragments.[46]

(37) Kirste, B.; van Willigen, H. *J. Phys. Chem.* **1982**, *86*, 2743–2749.
(38) Mulks, C. F.; Kirste, B.; van Willigen, H. *J. Am. Chem. Soc.* **1982**, *104*, 5906–5911.
(39) Gerfen, G. J.; Hanna, P. M.; Chasteen, N. D.; Singel, D. J. *J. Am. Chem. Soc.* **1991**, *113*, 9513–9519.
(40) Tipton, P. A.; McCracken, J.; Cornelius, J. B.; Peisach, J. *Biochemistry* **1989**, *28*, 5720–5728.
(41) Eaton, S. S.; Dubach, J.; More, K. M.; Eaton, G. R.; Thurman, G.; Ambruso, D. R. *J. Biol. Chem.* **1989**, *264*, 4776–4781.
(42) de Boer, E.; Keijzers, C. P.; Klaasen, A. A. K.; Reijerse, E. J.; Collison, D.; Garner, C. D.; Wever, R. *FEBS Lett.* **1988**, *235*, 93–97.
(43) Berry, R. S. *J. Chem. Phys.* **1960**, *32*, 933–938.
(44) For reviews concerning pentacoordination, see: (a) Rossi, A. R.; Hoffmann, R. *Inorg. Chem.* **1975**, *14*, 365–374. (b) Holmes, R. R. *Prog. Inorg. Chem.* **1984**, *32*, 119–235.
(45) Sheldrick, G. M. *SHELX 86, Crystal Structure Analysis Package*; University of Cambridge, England, 1986.

Spectroscopy. X-band CW EPR experiments were performed on a E-90 Varian spectrometer. Pulsed X-band EPR and ENDOR spectra were recorded with a homebuilt spectrometer (at ETH Zürich)[47] equipped with a bridged loop-gap resonator.[48] In the pulsed ENDOR experiments, the microwave (mw) resonator is surrounded by a solenoidal radio frequency (rf) coil that generates the rf field and serves as a mw radiation shield.[49]

The pulse scheme used in the ENDOR experiments[19] consists of the stimulated electron spin-echo sequence, $\pi/2 - \tau - \pi/2 - T - \pi/2 - \tau -$ echo, with nonselective mw pulses and a selective rf pulse of variable frequency ν_{rf} and flip angle $\beta_{rf} = \pi$ applied between the second and third mw pulses (Mims-ENDOR). The following parameters were used: length of the mw $\pi/2$ pulses, $t_{\pi/2} = 30$ ns; length of the rf π pulse, $t_{rf} = 40$ μs; rf increment, $\Delta\nu_{rf} = 10$ kHz; time between the first and second mw pulse, $\tau = 500$ ns ($g_\parallel$) and $\tau = 800$ ns ($g_\perp$); pulse repetition rate, 500 Hz.

In the electron spin-echo envelope modulation (ESEEM) experiments, both the two-pulse sequence, $\pi/2 - \tau - \pi - \tau -$ echo, and the three-pulse sequence, $\pi/2 - \tau - \pi/2 - T - \pi/2 - \tau -$ echo, with pulse lengths $t_{\pi/2} = 10$ ns and $t_\pi = 20$ ns were used. The time (τ in the two-pulse, T in the three-pulse experiment) was increased in increments of $\Delta t = 10$ ns, and time τ in the three-pulse ESEEM was fixed to 200-300 ns. ENDOR and ESEEM signals were recorded at temperatures between 10 and 20 K using a helium gas cooling system. Note that resonators with slightly different resonance frequencies have been used for the different experiments; the nuclear Zeeman frequencies of the ENDOR and ESEEM spectra may therefore not be determined from the EPR spectrum shown in Figure 4.

For the ENDOR measurements, deoxygenated toluene or toluene-d_8 solutions containing **1** (0.02 M) and α-^{13}C-benzaldehyde (99.6 atom % ^{13}C) or benzaldehyde-d_5 respectively (0.1 M; both purchased from Stohler Isotope Chemicals) were used. For the ESEEM studies, deoxygenated toluene solutions containing **1** (0.02 M) and *N*-benzylidene-benzylamine (0.1 M) were prepared.

The zero-frequency component in the time domain ESEEM data was eliminated by subtracting a fitted exponential. For cosine-Fourier transform spectra, the deadtime artifacts were reduced prior to transformation by tapering the ESEEM patterns with a shifted hanning window.

Supplementary Material Available: Tables of bond distances and angles, atomic coordinates, and isotropic thermal parameters; a table collecting bonding parameters for the fragment M-O-C in X-ray characterized complexes containing η^1-coordinated aldehydes, ketones, and esters (including literature references) (7 pages); listings of observed and calculated structure factors (8 pages). Ordering information is given on any current masthead page.

(46) For a selection of compounds containing disordered fluorinated substituents, see, e.g.: (a) Lindoy, L. F.; Lip, H. C.; Louie, H. W.; Drew, M. G. B.; Hudson, M. J. *J. Chem. Soc., Chem. Commun.* **1977**, 778-780. (b) Felthouse, T. R.; Dong, T.-Y.; Hendrickson, D. N.; Shieh, H.-S.; Thompson, M. R. *J. Am. Chem. Soc.* **1986**, *108*, 8201-8214. (c) Kamil, W. A.; Bond, M. R.; Willett, R. D.; Shreeve, J. M. *Inorg. Chem.* **1987**, *26*, 2829-2833. (d) Churchill, M. R.; Fennessey, J. P. *Inorg. Chem.* **1967**, *6*, 1213-1220.

(47) Schweiger, A. In *Modern Pulsed and Continuous Wave Electron Spin Resonance*; Kevan, L., Bowman, M. K.; Eds.; Wiley: New York, 1990.

(48) Pfenninger, S.; Forrer, J.; Schweiger, A.; Weiland, T. *Rev. Sci. Instrum.* **1988**, *59*, 752-760.

(49) Forrer, J.; Pfenninger, S.; Eisenegger, J.; Schweiger, A. *Rev. Sci. Instrum.* **1990**, *61*, 3360-3367.

Spectroscopic Detection and Reactivity of the Chlorine Atom-Carbon Disulfide Molecular Complex

John E. Chateauneuf

Contribution from the Radiation Laboratory, University of Notre Dame, Notre Dame, Indiana 46556. *Received June 4, 1992*

Abstract: Pulse radiolysis and laser flash photolysis techniques have been used to generate and kinetically characterize the chlorine atom-carbon disulfide molecular complex ($Cl^\bullet/CS_2$) in CCl_4 solution. The transient absorption spectrum of $Cl^\bullet/CS_2$ has been generated from three independent $Cl^\bullet$ sources: pulse radiolysis of CCl_4, 266-nm photodecomposition of CCl_4, and photodissociation of Cl_2. An absolute rate constant of 1.7×10^{10} M^{-1} s^{-1} for the reaction of $Cl^\bullet + CS_2$ was obtained from both the direct measurement of the decay of the charge-transfer band of $Cl^\bullet$ in CCl_4 ($\lambda_{max} = 330$ nm) and from the formation kinetics of $Cl^\bullet/CS_2$ ($\lambda_{max} = 370$ nm; shoulder = 490 nm). The properties of $Cl^\bullet/CS_2$ are compared with those of the molecular complexes of $Cl^\bullet$ with benzene and pyridine. The reactivity observed monitoring the $Cl^\bullet/CS_2$ absorption band toward 2,3-dimethylbutane has also been investigated to determine the equilibrium constant (K) of the $Cl^\bullet/CS_2$ complex, and the value of K is compared to that determined by direct spectroscopic method. K for the $Cl^\bullet$/pyridine complex has also been reevaluated.

Introduction

Recently, the gas-phase reaction of chlorine atom with carbon disulfide has received considerable attention[1-3] due to its potential importance in atmospheric chemistry. Both the relative rate technique[1,2] and time-resolved fluorescence[3] of chlorine atom have been used to determine that chlorine atom forms a reversible adduct with carbon disulfide.

The importance of the interaction of chlorine atom with carbon disulfide in liquid-phase photochlorination reactions was first reported by Russell.[4-6] Dramatic increases in selectivity in tertiary to primary hydrogen-atom abstractions were observed in the photochlorination of 2,3-dimethylbutane (DMB) in the presence of carbon disulfide[7] or benzene.

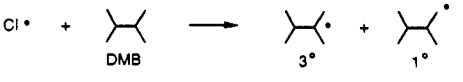

(1)

In the latter case, it is now generally believed that the enhanced tertiary to primary selectivity is a direct consequence of a rapidly formed chlorine atom-benzene π-molecular complex[8,9] (**1**). The

(1) Martin, D.; Barnes, I.; Becker, K. H. *Chem. Phys. Lett.* **1987**, *140*, 195-199.

(2) Wallington, T. J.; Andino, J. M.; Potts, A. R. *Chem. Phys. Lett.* **1991**, *176*, 103-108.

(3) Nicovich, J. M.; Shackelford, C. J.; Wine, P. H. *J. Phys. Chem.* **1990**, *94*, 2896-2903.

(4) Russell, G. A. *J. Am. Chem. Soc.* **1957**, *79*, 2977-2978.

(5) Russell, G. A. *J. Am. Chem. Soc.* **1958**, *80*, 4987-4996.

(6) Russell, G. A. *J. Am. Chem. Soc.* **1958**, *80*, 4997-5001.

(7) Also see: Skell, P. S.; Baxter, H. N.; Taylor, C. K. *J. Am. Chem. Soc.* **1983**, *105*, 120-121.

0002-7863/93/1515-1915$04.00/0